Electron *g* factor anisotropy in asymmetric III–V semiconductor quantum wells

2016 Semicond. Sci. Technol. 31 115008

(http://iopscience.iop.org/0268-1242/31/11/115008)

IOP Publishing Semiconductor Science and Technology
Semicond. Sci. Technol. 31 (2016) 115008 (7pp) doi:10.1088/0268-1242/31/11/115008

Electron *g* factor anisotropy in asymmetric III–V semiconductor quantum wells

M A Toloza Sandoval[1], E A de Andrada e Silva[1,4], A Ferreira da Silva[2] and G C La Rocca[3]

[1] Instituto Nacional de Pesquisas Espaciais, C.P. 515, 12201-970 São José dos Campos, São Paulo, Brazil
[2] Instituto de Física, Universidade Federal da Bahia 40210-340, Salvador, Bahia, Brazil
[3] Scuola Normale Superiore and CNISM, Piazza dei Cavalieri 7, I-56126 Pisa, Italy

E-mail: edeandrada@gmail.com

Received 24 May 2016, revised 19 July 2016
Accepted for publication 1 August 2016
Published 27 September 2016

Abstract

The electron effective *g* factor tensor in asymmetric III–V semiconductor quantum wells (AQWs) and its tuning with the structure parameters and composition are investigated with envelope-function theory and the 8×8 $\mathbf{k}\cdot\mathbf{p}$ Kane model. The spin-dependent terms in the electron effective Hamiltonian in the presence of an external magnetic field are treated as a perturbation and the *g* factors $g_\perp^*$ and $g_\parallel^*$, for the magnetic field in the QW plane and along the growth direction, are obtained analytically as a function of the well width *L*. The effects of the structure inversion asymmetry (SIA) on the electron *g* factor are analyzed. For the *g*-factor main anisotropy $\Delta g = g_\perp^* - g_\parallel^*$ in AQWs, a sign change is predicted in the narrow well limit due to SIA, which can explain recent measurements and be useful in spintronic applications. Specific results for narrow-gap AlSb/InAs/GaSb and $Al_xGa_{1-x}As/GaAs/Al_yGa_{1-y}As$ AQWs are presented and discussed with the available experimental data; in particular InAs QWs are shown to not only present much larger *g* factors but also a larger *g*-factor anisotropy, and with the opposite sign with respect to GaAs QWs.

Keywords: electron *g* factor, semiconductor quantum wells, spin–orbit interaction

(Some figures may appear in colour only in the online journal)

1. Introduction

Electron *g*-factor engineering, i.e. tuning the effective *g* factor (g^*) with quantum confinement effects in semiconductor nanostructures is of great interest to semiconductor spintronics [1–3]. g^* is a fundamental parameter that determines the Zeeman splitting of the electronic states and depends on different quantum effects. For the most basic example, in GaAs/AlGaAs like quantum wells (QWs) the *g* factor is determined by the confined wave-function and by the mesoscopic (Rashba type) spin–orbit (SO) interaction at the interfaces [4–7]. Breaking of translation symmetry along the QW growth direction ($\hat{z}$) leads to an electron (leading-order) *g*-factor tensor in the following form:

$$g_{\rm QW}^* = \begin{pmatrix} g_\perp^* & 0 & 0 \\ 0 & g_\perp^* & 0 \\ 0 & 0 & g_\parallel^* \end{pmatrix}, \qquad (1)$$

where $g_\perp^*$ gives the Zeeman splitting for magnetic field in the QW (i.e. *xy*) plane and $g_\parallel^*$ for $\vec{B}\|\hat{z}$. The difference $\Delta g = g_\perp^* - g_\parallel^*$ is the QW *g*-factor anisotropy, which in first order perturbation theory and for symmetric QWs with barriers at $z = \pm L/2$, reads [6]

$$\Delta g = \frac{4m_e}{\hbar^2}\,(\beta_w - \beta_b)\,L\,|f^{(0)}(L/2)|^2, \qquad (2)$$

$f^{(0)}$ being the unperturbed confined wave-function and β the (energy-dependent) Rashba SO coupling parameter, discussed below; with $g_\parallel^* = \bar{g}_{\rm bulk} = \langle f^{(0)}|g_{\rm bulk}|f^{(0)}\rangle$ (i.e. equals to the

[4] Author to whom any correspondence should be addressed.

bulk average). The g-factor anisotropy is then proportional to the difference between the βs in the well and in the barrier, and to the amplitude squared of the wave-function at the interface; and as a function of L (as shown later in figures 3 and 4), Δg is seen to start equals to zero at $L = 0$, to reach then an extremum (e.g. a maximum at $L \sim 4$ nm for GaAs QWs) and then to return slowly to zero as L goes to infinity.

These theoretical results for $g^*_{\rm QW}(L)$ give a simple picture for the renormalization of the electron g factor due to quantum confinement effects in III–V semiconductor QWs, are in good agreement with the experimental data for GaAs QWs [8–13], but are limited to symmetric QWs. The well known Ivchenko and Kiselev framework for the g-factor calculation [4, 14, 15] which is also based on the Kane model and envelope function approximation, presents an accurate solution for a general confinement (i.e. for both symmetric and asymmetric QWs) and was explicitly applied in biased GaAs and InGaAs triangular QWs [16]. However, the above perturbative solution is much simpler, gives an intuitive and useful physical interpretation for the g-factor renormalization, derives from long used and tested approximations in similar problems [17], more recently the g-factor solution has been applied also to PbTe QWs [7], GaN QWs [18] and GaAs nanodisks [3] and therefore it would be highly desirable to have such a solution for a general nanostructure. In particular, asymmetric quantum wells (AQWs), i.e. QWs with structure inversion asymmetry (SIA), are important candidates for structures with large g-factor variation. It is still not clear, for example, how the SIA affects the above results for the g factor in typical III–V AQWs. In this work we consider square AQWs (i.e. QWs with different left and right barriers), focus on the small L limit where both the quantum and SIA effects are larger, and extend the above solution for $g^*_{\rm QW}(L)$ to the case of AQWs. Such low field perturbation solution has shown to be accurate in the $L \to 0$ limit [6, 9–11], and reveal here an interesting g-factor anisotropy sign change in narrow AQWs that can be useful in different spintronic applications; a detailed derivation of the main results is provided.

It is also interesting to investigate the electron g factor in narrow-gap III–V semiconductor QWs with larger bulk g factors, stronger SO interaction and smaller remote-bands contribution than GaAs QWs. Among the narrow gap III–V semiconductors, InAs presents large SO interaction, high electron mobilities, small Shottky barriers and is therefore particularly attractive for spintronic applications [19, 20]. The gate-controlled electron g factor has been studied using InAs AQWs [2]. Here we consider the $g^*_{\rm QW}$ for electrons confined in undoped AlSb/InAs/GaSb AQWs. These are QW structures with SIA, analytical spin-split electronic structure and therefore of interest to the physics of Rashba coupling in semiconductor 2DEGs; the special possibilities connected with the type II band-alignment in one interface and type III in the other make them of interest also to the topological insulator physics [21, 22]. Here expressions for the electron $g^*_{\rm QW}(L)$ in general III–V square AQWs are obtained and used to calculate the electron g factor in specific InAs and GaAs AQWs. Several differences are found between them and between symmetric and asymmetric QWs; for example, the g-factor anisotropy Δg is seen to have opposite signs in InAs and GaAs QWs and, differently to the symmetric case, to change sign in narrow AQWs due to SIA.

Next we present the multi-band envelope-function model, then the AQW g-factor calculation, the results for GaAs and InAs AQWs, the comparison with the experiments and finally, in the conclusions, the summary of the results.

2. Multi-band envelope-function model

Using standard envelope-function method based on the 8×8 $\mathbf{k}\cdot\mathbf{p}$ Kane model for the bulk, the set of equations for the envelope functions can be written as an effective Hamiltonian for the electron (i.e. conduction band (CB)) envelope-functions, with energy dependent effective-mass and explicit Rashba SO coupling [23–25]. In the presence of an external magnetic field we follow [6], add the bare Zeeman interaction, make the fundamental substitution $\mathbf{k} \to \mathbf{k} + \frac{e}{\hbar}\mathbf{A}$ ($-e$ being the electron charge) and, as further explained in the appendix, obtain the following effective Hamiltonian for the QW electronic states in an in-plane magnetic field $\mathbf{B} = (0, B, 0)$:

$$H^{(\sigma)}_{\rm eff} = -\frac{\hbar^2}{2}\frac{\rm d}{{\rm d}z}\frac{1}{m(z,\varepsilon_\sigma)}\frac{\rm d}{{\rm d}z} + \frac{\hbar^2}{2}\frac{[(z-z_0)/\ell^2]^2}{m(z,\varepsilon_\sigma)} + E_c(z) \mp \frac{2m_e}{\hbar^2}[\alpha(z,\varepsilon_\sigma)(z-z_0)+\beta(z,\varepsilon_\sigma)]\mu_B B, \tag{3}$$

where the CB edge profile $E_c(z)$ is now a general one. The Landau gauge is used with vector potential $\mathbf{A} = (z\,B, 0, 0)$ and the signs $\mp$ stand for spin down or up along $\hat{y}$. Note that with this gauge the envelope function can be written as $\Psi = {\rm e}^{{\rm i}(k_x x + k_y y)} f(z)$, with $f(z)$ satisfying $H^{(\sigma)}_{\rm eff} f = \varepsilon_\sigma f$, k_x being a quantum number that gives the center of the cyclotron orbit, i.e. $z_0 = -\ell^2 k_x$, where $\ell = \sqrt{\hbar/eB}$ is the magnetic length; and k_y is the wave-vector for the free motion along the B-field direction which is zero for the ground-state. Finally ε_σ is the electron energy with spin σ ($=\pm$), the Bohr magneton $\mu_B = e\hbar/2m_e$ (m_e being the free-electron mass), $\alpha(z,\varepsilon_\sigma) = \frac{\rm d}{{\rm d}z}\beta(z,\varepsilon_\sigma)$ and the effective mass $m(z,\varepsilon_\sigma)$ and Rashba SO parameter $\beta(z,\varepsilon_\sigma)$ are given by:

$$\frac{1}{m(z,\varepsilon_\sigma)} = \frac{P^2}{\hbar^2}\left[\frac{2}{\varepsilon_\sigma - E_v(z)} + \frac{1}{\varepsilon_\sigma - E_v(z) + \Delta(z)}\right] \tag{4}$$

and

$$\beta(z,\varepsilon_\sigma) = \frac{P^2}{2}\left[\frac{1}{\varepsilon_\sigma - E_v(z)} - \frac{1}{\varepsilon_\sigma - E_v(z) + \Delta(z)}\right], \tag{5}$$

where E_v and Δ stand for the material valence band (VB) edge and SO splitting respectively; $P = -{\rm i}(\hbar/m_e)\sqrt{\frac{2}{3}}\,\langle S|p_x|X\rangle$ is the momentum matrix element, assumed constant along the structure (as a fundamental assumption of the envelope-function approximation) and determined by the measured CB edge effective-mass in the well m^*, i.e. $P = \sqrt{\frac{\hbar^2}{m^*}\frac{E_g(E_g+\Delta)}{3E_g+2\Delta}}$. It is easy to test and verify that the above effective Hamiltonian

reduces exactly to well-known Hamiltonians in three limits: (1) in the zero magnetic field limit, giving the usual model for the Rashba effect [23–25], (2) with no SO interaction, giving the regular Landau level quantization in a QW [26] and (3) in the bulk limit, reducing to the theory of Roth *et al* [27] for the energy-dependent bulk g factor.

3. The *g* factor in AQWs

The ground state $g^*_{\rm QW}$ can be calculated in the small magnetic-field limit considering the spin dependent terms in $H^{(\sigma)}_{\rm eff}$ as a perturbation. The zeroth order wave-function $f^{(0)}(z)$ and energy ε_0 are solutions of the unperturbed problem, i.e. with $B=0$ and $k_y=k_x=0$, $\left(-\frac{\hbar^2}{2}\frac{\rm d}{{\rm d}z}\frac{1}{m(z,\varepsilon_\sigma)}\frac{\rm d}{{\rm d}z}+E_c(z)\right)f^{(0)}(z)=\varepsilon_0 f^{(0)}(z)$, which corresponds to the Kane AQW problem, which in turn can be easily solved exactly [25]. However, differently to the case of a symmetric QW, the expectation value $\bar z$ does not coincide in general with the center of the well. For symmetric QWs with barriers at $z=\pm L/2$, $\bar z=0$ and thus the lowest energy state also has $z_0=0$ (i.e., $k_x=0$). For AQWs instead, z_0 has to be calculated minimizing the term $\frac{\hbar^2}{2m(z,\varepsilon_\sigma)}[(z-z_0)/\ell^2]^2$ in $H^{(\sigma)}_{\rm eff}$ which simply leads to $z_0=\bar z$, independent on B (while $k_x\propto B\,z_0$ still vanishes when $B\to 0$). We note that an alternative approach would be to change both coordinates, using $z'=z-\bar z$, and gauge, using $\mathbf{A}'=(z'B,0,0)$, in which case the wave function changes as $\Psi\to\Psi'=e^{ie\bar zBx/\hbar}\Psi$ and the lowest energy Ψ' would correspond to $z_0'=0$ and $k_x'\equiv 0$. Focussing here on AQWs, we prefer to leave the role played by $\bar z$ explicit, which accounts for the diamagnetic shift [14–16].

In first order perturbation theory, one can simply calculate the g factor from equation (3) as:

$$g^*_\perp = \bar g_{\rm bulk} - \frac{4m_e}{\hbar^2}\langle f^{(0)}|\alpha_R(z,\varepsilon_0)(z-\bar z)|f^{(0)}\rangle. \tag{6}$$

Note that in flat-band wells α_R $(=\frac{\rm d}{{\rm d}z}\beta)$ is different from zero only at the interfaces where β changes abruptly. With $\vec B\|\hat z$, the system recovers the rotation symmetry around to growth direction, and in the same approximation (see appendix) $g^*_\parallel$ is given by the bulk average, i.e.

$$g^*_\parallel = \bar g_{\rm bulk} = g_e + \langle f^{(0)}|-\frac{4m_e}{\hbar^2}\beta(z,\varepsilon_0)+\delta g_{\rm rem}(z)|f^{(0)}\rangle, \tag{7}$$

$\delta g_{\rm rem}$ being the difference between the g-factor measured experimentally and that given by the Roth formula, i.e. the remote-bands contribution [27], and g_e the free electron g factor equals to 2. The QW g-factor anisotropy is then given simply by:

$$\Delta g = g^*_\perp - g^*_\parallel = -\frac{4m_e}{\hbar^2}\langle f^{(0)}|\alpha_R(z,\varepsilon_0)(z-\bar z)|f^{(0)}\rangle. \tag{8}$$

As illustrated in figure 1, for a general III–V square AQW we set the two non-equivalent interfaces at $z=z_l$ and $z=z_r$, with $z_r-z_l=L$. The expectation values above can be easily calculated and one gets:

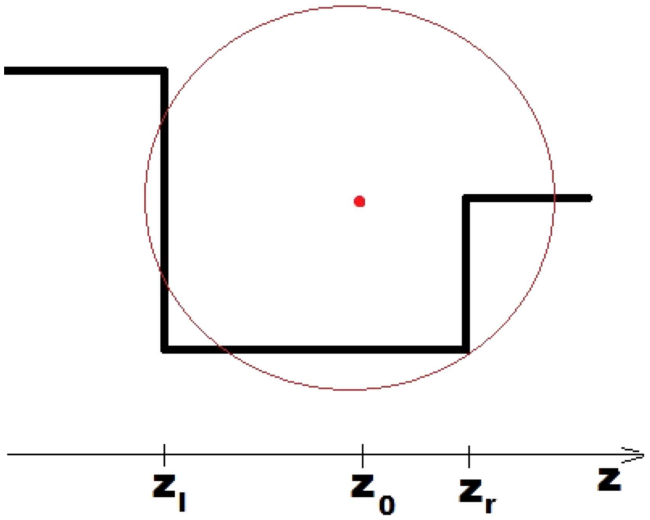

Figure 1. Schematic illustration of a square asymmetric QW grown along z with different interfaces at z_l and z_r, and of the classical cyclotron orbit in real space for in-plane magnetic fields, centered at z_0.

$$g^*_\parallel = g_l(\varepsilon_0)P_l + g_w(\varepsilon_0)P_w + g_r(\varepsilon_0)P_r \tag{9}$$

and

$$\Delta g = (\Delta g)_r - (\Delta g)_l, \tag{10}$$

where P_i $(=\int_i |f^{(0)}(z)|^2{\rm d}z)$ is the probability to find the electron in the region i ($i=l$ for $z\leqslant z_l$, $i=w$ for $z_l<z<z_r$ and $i=r$ for $z\geqslant z_r$); the bulk g factors $g_i=g_e-\frac{4m_e}{\hbar^2}\beta_i(\varepsilon_0)+\delta g^{(i)}_{\rm rem}$ and

$$(\Delta g)_j = \frac{4m_e}{\hbar^2}\delta\beta_j(z_j-\bar z)|f^{(0)}(z_j)|^2 \tag{11}$$

with $j=l,r$ and $\delta\beta_j=\beta_w-\beta_j$.

The g-factor anisotropy Δg in AQWs is then seen to be determined by the differences $\delta\beta$ and by the wave-function amplitudes (squared) at each interface, weighted however by their distance to the center of the ground state orbit $z_0=\bar z$. Note that in symmetric QWs $\delta\beta_l=\delta\beta_r$, $\bar z-z_l=z_r-\bar z=L/2$ and the symmetrical result in equation (2) is recovered. Recall also that for symmetric QWs, the ground-state corresponds to $\bar z=(z_l+z_r)/2$ at the center of the well and the contributions from the two interfaces are equal: $-(\Delta g)_l=(\Delta g)_r=\Delta g/2$. The specific contribution of the SIA to Δg increases with $|(z_l+z_r)/2-\bar z|$ and with $|\delta\beta_r|f^{(0)}(z_r)|^2-\delta\beta_l|f^{(0)}(z_l)|^2|$. It is interesting to consider also the limit case of an infinite high barrier (a perfect insulator) in one of the two sides (say the l side); in this case, the g factor anisotropy is simply given by $\Delta g=\frac{4m_e}{\hbar^2}\delta\beta_r(z_r-\bar z)|f^{(0)}(z_r)|^2$.

Contrary to the symmetric QW case, the sign of Δg in AQWs is not uniquely determined by the sign of $\delta\beta$ but depends also on the sing of $(z_{\rm interf}-\bar z)$. In practice, to calculate $g^*_{\rm QW}(L)$ one solves the unperturbed problem and in the above equations just plug in the obtained $f^{(0)}_L(z)$, $\varepsilon_0(L)$ and

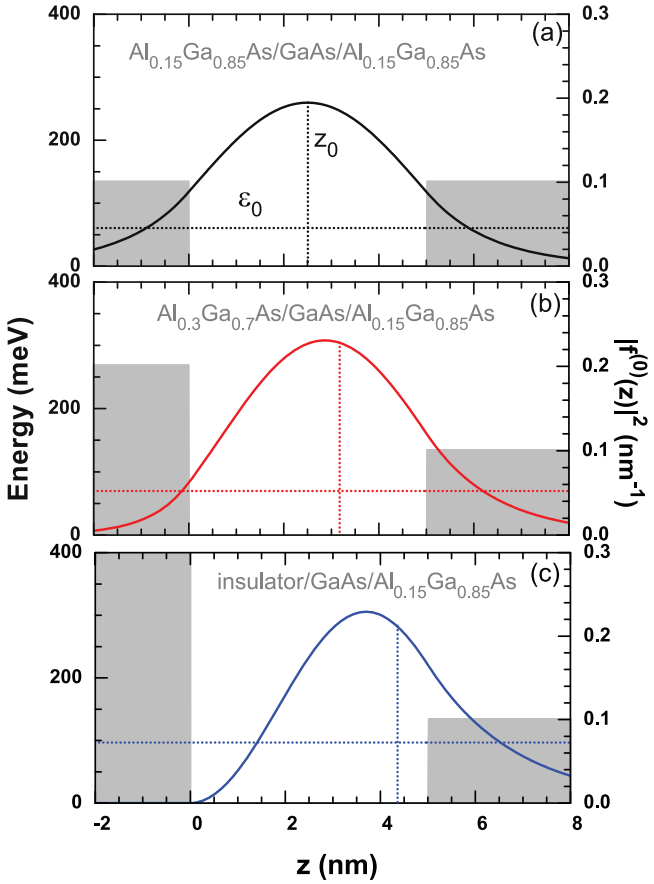

Figure 2. Conduction band-edge profile $E_c(z)$, ground state energy ε_0 and probability density $|f^{(0)}(z)|^2$ (with axis on the right) for $L = 5$ nm (a) $Al_{0.15}Ga_{0.85}As/GaAs/Al_{0.15}Ga_{0.85}As$ SQW, (b) $Al_{0.3}Ga_{0.7}As/GaAs/Al_{0.15}Ga_{0.85}As$ AQW (red lines) and (c) insulator/GaAs/$Al_{0.15}Ga_{0.85}As$ AQW (blue lines). The respective ground state orbit centers $z_0 = \bar{z}$ are also shown. The parameters used were $E_g = (1.519 + 1.247x)$ eV, $\Delta = (1.859 + 1.115x + 0.37x^2 - E_g)$ eV (x being the Al concentration) and 0.067 m_e for the GaAs conduction-band edge effective mass. For the conduction band-offset the 72% rule was used.

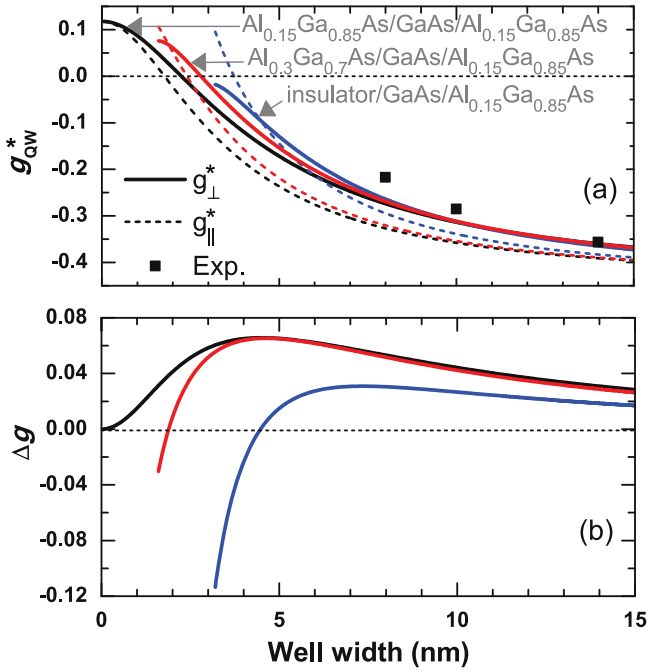

Figure 3. Effective electron g factors and the anisotropy Δg as a function of the well width, in panels (a) and (b) respectively, for the same structures in figure 2. In AQWs, Δg is seen to change sign for narrow wells; note that the curves stop at the corresponding critical well width for a bound state. A bulk conduction-band edge $g^* = -0.44 + 4.25x - 3.9x^2$ (x being the Al concentration) was used [28]. The experimental points are for $g_\parallel^*$ in asymmetrically doped GaAs/$Al_{0.15}Ga_{0.85}As$ AQWs as reported in [29].

also $\bar{z}(L)$. Next we discuss the results for specific GaAs and InAs AQWs.

4. $Al_xGa_{1-x}As/GaAs/Al_yGa_{1-y}As$ AQW

As a first example we consider $Al_xGa_{1-x}As/GaAs/Al_yGa_{1-y}As$ (with $x \neq y$) AQWs. The results for $g^*_{QW}(L)$ in these wells are compared to those in similar GaAs symmetric wells (SQWs) and in insulator/GaAs/$Al_yGa_{1-y}As$ AQWs. Typical ground-state unperturbed solutions for these three types of QWs are shown in figure 2 with the CB profile and $L = 5$ nm, showing that the wave-function is deformed and z_0 is pushed away from the barrier on the left as the barrier height increases. Similarly, for a fixed AQW profile, z_0 is pushed away from the higher barrier as the well width L is decreased.

In figure 3, the obtained $g_\perp^*$, $g_\parallel^*$ and Δg for these three wells are plotted as a function of L. First it is interesting to see that the break of specular symmetry (or SIA) has only small quantitative effects in the GaAs QW electron g factor except for narrow wells when the g-factor anisotropy changes sign and starts to increase rapidly. In these GaAs square AQWs there is always a critical well width below which $g_\perp^*$ becomes smaller than $g_\parallel^*$, i.e. Δg becomes negative, while in symmetric QWs Δg is always positive. Such anisotropy sign change in thin AQWs is due to the $\bar{z}$ dependence. For example, in insulator/GaAs/GaAlAs AQWs it happens when $\bar{z} > z_r$, i.e. when the expectation value of the electron position along the growth direction lies outside the QW or GaAs region. Note also that for large well widths, the anisotropy of the $Al_xGa_{1-x}As/GaAs/Al_yGa_{1-y}As$ AQWs tend to that of the GaAs SQW, and when one of the barriers is infinitely high, the anisotropy is a factor of 2 smaller, as due to one interface only.

5. AlSb/InAs/GaSb AQW

The present 8×8 $\mathbf{k}\cdot\mathbf{p}$ Kane model is much more precise for InAs than it is for GaAs, as indicated by a much smaller $\delta g_{rem}/g$, which is ~0.03 for InAs and ~1.1 for GaAs. Here we consider the electron g factor in InAs QWs similar to the GaAs ones discussed above, namely thin InAs/GaSb symmetric QWs, AlSb/InAs/GaSb AQWs and insulator/InAs/GaSb AQWs. Due to the broken-gap band alignment,

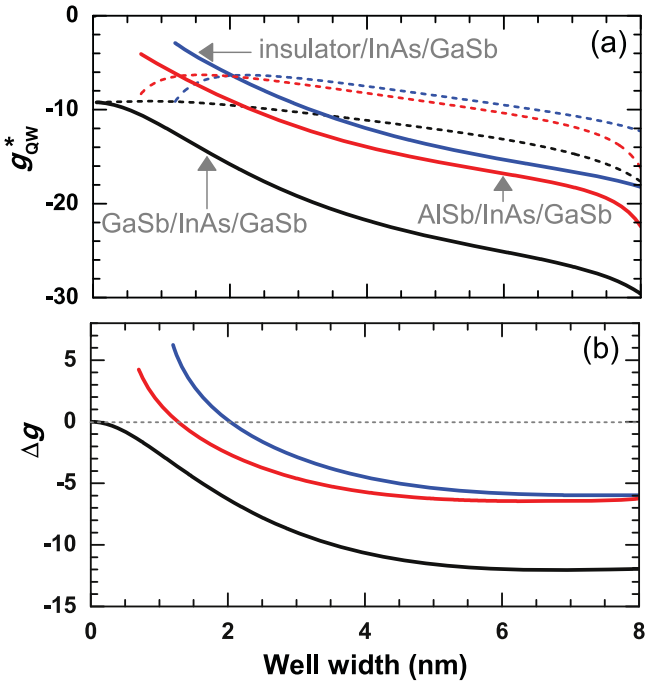

Figure 4. Effective electron g factors ($g_\perp^*$, $g_\parallel^*$) and the corresponding anisotropy Δg (panels (a) and (b) respectively) as a function of the well width, for three different InAs QWs: GaSb/InAs/GaSb symmetric QW (black lines), insulator/InAs/GaSb asymmetric QW (blue lines) and AlSb/InAs/GaSb asymmetric QW (red lines). As before, dashed lines give $g_\parallel^*$ and continuous $g_\perp^*$. Well known bulk low temperature parameters [32] and 0.96 eV and 1.98 eV for InAs/GaSb and InAs/AlSb conduction-band offsets respectively, were used.

there are InAs confined electron states in these QWs with GaSb barriers only when the well width $L < L_c \sim 9$ nm. This is because in InAs/GaSb QWs with $L > L_c$, the electron energy ε_0 gets below E_v^{GaSb} and the state is not confined in the InAs layer anymore [30, 31]. Note that when $\varepsilon_0 = E_v^{\mathrm{GaSb}}$, the GaSb (bulk) g factor diverges (see expression for β in equation (5)) and $g^*_{\mathrm{QW}}(L \sim L_c)$ is therefore expected to be quite large since the barrier penetration is also expected to increase when $L \to L_c$.

In figure 4(a) it is plotted the calculated $g_\perp^*$ (continuous lines) and $g_\parallel^*$ (dashed lines) for the three types of wells as a function of L; and in figure 4(b), the corresponding Δg. The SIA can be clearly seen to have a much stronger effect in InAs QW g factors than it has in GaAs wells, due to the stronger SO interaction. Compared to GaAs QWs, the electron g factor in InAs QWs is seen to be two-orders of magnitude larger, with Δg also much larger and of the opposite sign. Note that the anisotropy Δg in these InAs AQWs changes sign at a smaller well width and that in AlSb/InAs/GaSb wells, in the large L limit, Δg tend to that of insulator/InAs/GaSb AQWs, instead to that of SQWs as in GaAs wells, due to the large conduction (Γ) AlSb/InAs band-offset. In these InAs AQWs, $g_\parallel^*$ is seen to present a maximum as a function of L.

It is also interesting to note the obtained large (in absolute value) electron g factor (~30) in InAs/GaSb QWs when $L \to L_c$, which as just discussed, is due to barrier penetration and to a divergence in the energy dependence of the bulk g factor in GaSb. We now compare these calculations with the available experimental data.

6. Comparison with the experiments

The electron g factor in GaAs/AlGaAs symmetric QWs has been measured by different groups using both optical and transport techniques, involving time-resolved photoluminescence and magnetoresistance measurements [8–13]. In particular $g_\parallel^*$ is now well known; with good accuracy, it is given by the above QW average of the bulk g factors, which includes effects from the energy dependence of the bulk g factors and from the wave-function barrier penetration. Shown in figure 3(a), as L goes from very large values to near zero, $g_\parallel^*$ interpolates from the g factor in the well material to that in the barrier, with a sign change and, therefore, $g_\parallel^*=0$ for a certain (narrow) well [4, 13].

The anisotropy Δg and its well width dependence are less well known. With spin-quantum beats in the time-resolved photoluminescence [9], Le Jeune *et al* [10] and Malinowski and Harley [11] have measured $\Delta g\,(L)$ in GaAs symmetric QWs, and as shown in [6] it is simply and accurately described by equation (2) above. In $Al_xGa_{1-x}As/GaAs/Al_yGa_{1-y}As$ square AQWs, Ye *et al* [33] have measured the in-plane Zeeman splitting anisotropy which is allowed by the SIA but is due to higher order terms (in k and in B) [34].

More recently, $g^*_{\mathrm{QW}}(L)$ in asymmetrically doped GaAs/AlGaAs AQWs was studied by Shchepetilnikov *et al* [29] using electron spin resonance detected with magnetoresistance measurements. These data with doped AQWs can not be precisely compared with our undoped square AQW results; nevertheless, as shown in figure 3(a), the observed values and well width dependence of $g_\parallel^*$ agree fairly well with the theory. As expected the experimental $g_\parallel^*$ (which is for doped, $\varepsilon_F \neq 0$, AQWs) is a little larger than the calculated one (which is for undoped wells); more interesting, the measured g-factor anisotropy $\Delta g \sim 0.08$ for the 8 nm AQW (see [29] figure 3) is not far from the calculated $\Delta g = 0.05$ in figure 3(b) above (note that in such well width range, both $g_\parallel^*$ and Δg increase with electron energy).

In such GaAs AQWs, there are also measurements of the g-factor sign-reversal well-width L_0 [13] and of the g-factor dependence on the barrier height, controlled by the Al concentration x [29], which can further test of our model. A $L_0 = 6.5 \pm 0.3$ nm was determined for a $GaAs/Al_{x=0.33}GaAs$ asymmetrically doped QW and in figure 5 it is shown that a L_0 very close to that is expected also theoretically, considering the above mentioned shift due to the non zero Fermi energy. The figure compares our results for $g_\parallel^*(L)$ in both symmetric and asymmetric (with infinite

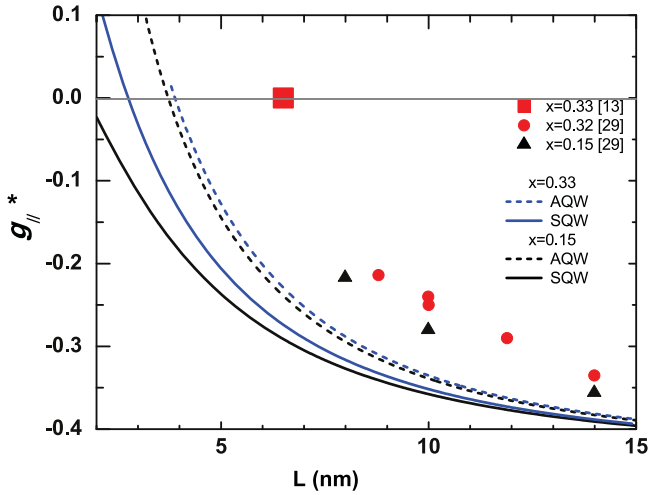

Figure 5. Longitudinal effective electron g factor ($g_{\parallel}^*$) as a function of the well width, for both symmetric and asymmetric (i.e., with infinite high left barrier) GaAs/GaAlAs QWs, with Al concentration $x = 0.15$ and 0.33. The measurements are from [13] and [29].

high left barrier) GaAs/$Al_xGa_{1-x}As$ QWs, with $x = 0.15$ and 0.33, and with the experimental data of [29]; one sees that L_0 increases with both x and SIA and that the model describes quantitatively well also the barrier height dependence, i.e. nearly the same difference with the same change in x is obtained both theoretical and experientaly. Note that this mesoscopic barrier-penetration effect on g^* applies to general nanostructures, independently of the microscopic details or structural defects. However, for a precise simulation of these doped structures for example, one has to consider the occupation of the states and the corresponding self-consistent electrostatic-field, which will require numerical solutions; but the equations to be used and the effects of the SO interaction at the interfaces are as described here. Nevertheless, measurements of Δg in thin undoped square AQWs would still be the best test of our model and of the predicted effect of anisotropy sign change.

Regarding such negative anisotropy in narrow GaAs AQWs, Tomimoto *et al* [35] have measured a negative Δg in a single sample with very narrow ($L = 0.32$ nm) CdTe/ZnTe QW and attributed it to a change in the sign of $\delta\beta$. It is interesting to note however that the g factor in such wells behaves as in GaAs QWs, with positive Δg and no change in the sign of $\delta\beta$ as a function of L when it is symmetric; this observed negative Δg is then likely to have another explanation. The growth of homogeneous and symmetric CdTe/ZnTe QWs is difficult due to the large lattice mismatch and the sample studied may well present some specular asymmetry which can account for the observed negative Δg.

For InAs QWs there are much fewer experimental data. Smith and Fang [36] measured an electron $g_{\rm QW}^* \sim -8$, in 10 nm GaSb/InAs/GaSb QWs, which however is a too wide QW, i.e. beyond the bound state regime considered here; and can not be compare with our results also due to the large magnetic fields employed in the coincidence (between Zeeman and Landau-level splittings) method used. The g factor in wide InAs QWs was determined with similar methods also in references [37, 38]. The electron g factor in thin InAs AQWs was studied by Nitta *et al* [2] and an $|g_{\parallel}^*|$ of the order of 3.5 was measured in biased 4 nm InAs/InGaAs AQWs, which is not far from the present results, however the structures are quite different and can not be directly compared. In general, a self-consistent treatment of the band-edge profile and/or a fine control of the structure parameters (including temperature dependence, precise band-offset and electron effective mass etc) are needed for a quantitative precise description of the experimental data. The anisotropy Δg in InAs QWs does not seem to have been measured yet.

7. Conclusions

Enough ground has been given to believe that the electron effective g factor in III–V semiconductor AQWs can be tuned within a wide range of values by controlling the well width and composition, including a change of sign in both g factor and g-factor anisotropy. The obtained effect of g-factor anisotropy sign change in narrow wells is shown to be due to SIA and determined by the electron average position in the AQW, and can explain recent observations. Results for the electron effective g factor tensor in different GaAs and InAs QWs have been presented in fairly good agreement with the available experimental data. With respect to GaAs QWs, InAs QWs are seen to not only have a much larger g factor and g-factor anisotropy but also opposite anisotropy sign. The analytical expressions derived apply to general III–V square AQWs and, as for the SQW case, can be easily extended to describe also IV–VI and GaN AQWs, for example. These results for the g-factor renormalization by the mesoscopic quantum confinement in semiconductor nanostructures should be of importance not only for the development of spintronic devices but also for the spin manipulation with external electric or magnetic fields in spin-based qubits made with semiconductor nanostructures.

Acknowledgments

EAAS is thankful to the Scuola Normale Superiore di Pisa, for the kind hospitality. Support from the brazilian agencies FAPESB/PRONEX, FAPESP (2014/09878-1, 2016/03845-9) and CNPq (303304/2010-3, 506194/2013-2 and 170145/2013-1) is also acknowledged.

Appendix. Effective Hamiltonian and g^* for III–V QWs

The effective Hamiltonian used for the QW electronic states in both transverse (equation (3)) and longitudinal magnetic fields, is obtained projecting the 8×8 Kane Hamiltonian into the 2×2 conduction-band space. Considering QWs grown along $\hat{z}$ and using the same basis states as in [24] after some simple algebra one obtains the following Schroedinger-Pauli-

like effective Hamiltonian:

$$H_{\text{eff}} = H_0 1 + \mathrm{i}\,[\beta(z,\varepsilon_\sigma)\hat{k}_x, \hat{k}_z]\sigma_y + \mathrm{i}\,\beta(z,\varepsilon_\sigma)[\hat{k}_x, \hat{k}_y]\sigma_z + \mathrm{i}\,[\beta(z,\varepsilon_\sigma)\hat{k}_y, \hat{k}_z]\sigma_x, \quad \text{(A.1)}$$

where H_0 is the usual spin-independent part, i.e. kinetic energy plus confining potential, with the energy dependent effective mass in equation (4). The components $\hat{k}_i$ are the momentum $(\mathbf{k} + \frac{e}{\hbar}\mathbf{A})$ operators, which for zero magnetic field lead to $\hat{k}_z = -\mathrm{i}\frac{\mathrm{d}}{\mathrm{d}z}$ plus $\hat{k}_x = k_x$ and $\hat{k}_y = k_y$ (i.e. good quantum numbers). Note that in this case one then has $[k_x, k_y] = 0$, $[\beta k_x, \hat{k}_z] = \mathrm{i}\,\alpha k_x$ and $[\beta k_y, \hat{k}_z] = \mathrm{i}\,\alpha k_y$ (recall that $\alpha = \frac{\mathrm{d}\beta}{\mathrm{d}z}$) which substituting above give the well known Rashba effective Hamiltonian [23–25] (with energy dependent SO coupling parameter α; note that β is sometimes also called Rashba coupling parameter, but clearly should not be confused with its derivative α).

In the presence of a longitudinal homogeneous magnetic field, one can use the Landau gauge $\mathbf{A} = (-By, 0, 0)$ and after the fundamental substitution finds $[\hat{k}_x, \hat{k}_y] = -\mathrm{i}\frac{e}{\hbar}B$, $[\beta\hat{k}_y, \hat{k}_z] = \mathrm{i}\,\alpha\hat{k}_y$ and $[\beta\hat{k}_x, \hat{k}_z] = \mathrm{i}\,\alpha\left(\hat{k}_x - \frac{e}{\hbar}By\right)$. Since in this case H_{eff} does not depend on x, one can write the envelope spinor as $\psi = \mathrm{e}^{\mathrm{i}k_x x}\psi(y, z)$, where k_x sets the center of the orbit and can be chosen equal to zero, and one then has:

$$H_{\text{eff}} = H_0 1 + \alpha\left(\hat{k}_y\sigma_x + \frac{e}{\hbar}By\sigma_y\right) + \beta\frac{e}{\hbar}B\sigma_z. \quad \text{(A.2)}$$

Note that independently of the known divergence of the vector potential in infinite systems (which can be treated with a modulated vector potential [15, 39] or by considering finite systems [14]), the off-diagonal terms above, i.e. those proportional to α are much smaller than the diagonal ones (proportional to β) and in a good first approximation can be neglected, so that $g_{\|}^{*}$ is simply given by equation (7). The accuracy of this approximation was verified in [4] where it is shown to be in close agreement with the full solution of the Kiselev–Ivchenko equations (see curves 1 and 3 in figure 3 there); the present approximation corresponds to neglecting the Kiselev–Ivchenko auxiliary function h [14, 15], which is indeed several orders of magnitude smaller than the main function. Note also that in the flat-band QWs considered here α is different from zero only at the two interfaces, where it presents opposite signs, so that the corresponding expectation values should indeed be very small compared with the main term.

Similarly for a transverse magnetic field, as already discussed, one can chose $\mathbf{A} = (Bz, 0, 0)$ and has $[\hat{k}_x, \hat{k}_y] = 0$, $[\beta\hat{k}_y, \hat{k}_z] = \mathrm{i}\,\alpha k_y$ and $[\beta\hat{k}_x, \hat{k}_z] = \mathrm{i}(\alpha\,(k_x + \frac{e}{\hbar}Bz) + \frac{e}{\hbar}\beta B)$, which substituting above give the effective Hamiltonian in equation (3).

References

[1] Kosaka H, Kiselev A, Baron F, Wook Kim K and Yablonovitch E 2001 *Electron. Lett.* **37** 464
[2] Nitta J, Lin Y, Akazaki T and Koga T 2003 *Appl. Phys. Lett.* **83** 4565
[3] Yang L-W, Tsai Y-C, Li Y, Higo A, Murayama A, Samukawa S and Voskoboynikov O 2015 *Phys. Rev.* B **92** 245423
[4] Ivchenko E L and Kiselev A A 1992 *Sov. Phys. Semicond.* **26** 827
[5] Pfeffer P and Zawadzki W 2006 *Phys. Rev.* B **74** 233303
[6] Toloza Sandoval M A, Ferreira da Silva A, de Andrada e Silva E A and La Rocca G C 2012 *Phys. Rev.* B **86** 195302
[7] Ridolfi E, de Andrada e Silva E A and La Rocca G C 2015 *Phys. Rev.* B **91** 085313
[8] Snelling M J, Flinn G P, Plaut A S, Harley R T, Tropper A C, Eccleston R and Phillips C C 1991 *Phys. Rev.* B **44** 11345
[9] Hannak R, Oestreich M, Heberle A, Ruhle W and Kohler K 1995 *Solid State Commun.* **93** 313
[10] Le Jeune P, Robart D, Marie X, Amand T, Brosseau M, Barrau J and Kalevcih V 1997 *Semicond. Sci. Technol.* **12** 380
[11] Malinowski A and Harley R T 2000 *Phys. Rev.* B **62** 2051
[12] Yugova I A, Greilich A, Yakovlev D R, Kiselev A A, Bayer M, Petrov V V, Dolgikh Y K, Reuter D and Wieck A D 2007 *Phys. Rev.* B **75** 245302
[13] Solov′ev V V, Dietsche W and Kukuskin I V 2014 *JETP Lett.* **100** 746
[14] Kiselev A A, Ivchenko E L and Rössler U 1998 *Phys. Rev.* B **58** 16353
[15] Kiselev A A, Kim K W and Ivchenko E L 1999 *Phys. Status Solidi* b **215** 235239
[16] Ivchenko E, Kiselev A and Willander M 1997 *Solid State Commun.* **102** 375
[17] Heisz J and Zaremba E 1993 *Semicond. Sci. Technol.* **8** 575
[18] Li M, Feng Z-B, Fan L, Zhao Y, Han H and Feng T 2016 *J. Magn. Magn. Mater.* **403** 81
[19] Datta S and Das B 1990 *Appl. Phys. Lett.* **56** 665
[20] Žutić I, Fabian J and Sarma S D 2004 *Rev. Mod. Phys.* **76** 323
[21] Knez I, Rettner C T, Yang S-H, Parkin S S P, Du L, Du R-R and Sullivan G 2014 *Phys. Rev. Lett.* **112** 026602
[22] Du L, Knez I, Sullivan G and Du R-R 2015 *Phys. Rev. Lett.* **114** 096802
[23] Gerchikov L G and Subashiev A V 1992 *Sov. Phys.- Semicond.* **26** 73
[24] de Andrada e Silva E A, La Rocca G C and Bassani F 1994 *Phys. Rev.* B **50** 8523
[25] de Andrada e E , La Rocca G and Bassani F 1997 *Phys. Rev.* B **55** 16293
[26] Brozak G, de Andrada e Silva E, Sham L, DeRosa F, Miceli P, Schwarz S, Harbison J, Florez L and Allen S Jr 1990 *Phys. Rev. Lett.* **64** 471
[27] Roth L M, Lax B and Zwerdling S 1959 *Phys. Rev.* **114** 90
[28] Weisbuc C and Herman C 1977 *Phys. Rev.* B **15** 816
[29] Shchepetilniko A, Nefyodov Y, Kukushkin I and Dietsche W 2013 *J. Phys.: Conf. Ser.* **456** 012035
[30] Altarelli M 1983 *Phys. Rev.* B **28** 842
[31] Yang M J, Yang C H, Bennet B R and Shanabroo B V 1997 *Phys. Rev. Lett.* **78** 4613
[32] Jancu J-M, de Andrada e Silva E A, Scholz R and Rocca G C La 2005 *Phys. Rev.* B **72** 193201
[33] Ye H, Hu C, Wang G, Zhao H, Tian H, Zhang X, Wang W and Liu B 2011 *Nanoscale Res. Lett.* **6** 520
[34] Kalevich V K and Korenev V L 1993 *JETP Lett.* **57** 571
[35] Tomimoto S, Nozawa S, Terai Y, Kuroda S, Takita K and Masumoto Y 2010 *Phys. Rev.* B **81** 125313
[36] Smith T P III and Fang F F 1987 *Phys. Rev.* B **35** 7729
[37] Yang M J, Wagner R J, Shanabrook B V, Waterman J R and Moore W J 1993 *Phys. Rev.* B **47** 6807
[38] Brosig S, Ensslin K, Jansen A G, Nguyen C, Brar B, Thomas M and Kroemer H 2000 *Phys. Rev.* B **61** 13045
[39] Luttinger J and Stiles P 1961 *J. Phys. Chem. Solids* **17** 284